Chapter 5

EMISSION AND DEPOSITION OF DUST BY WIND IN THE NELLIS DUNES RECREATION AREA

Dirk Goossens and Brenda Buck

Department of Geoscience, University of Nevada Las Vegas

1. Gross emission, net emission and gross deposition

This chapter describes the emission of dust generated by wind erosion in the Nellis Dunes Recreation Area (NDRA). Emissions were measured at 68 locations ("dust stations") installed on all 17 surface units that occur in the area. For practical applications and management issues it is essentially net emission (the difference in sediment mass, on the Earth's surface, before and after a time interval within which aeolian activity has taken place) that is of concern. Net emission is what is commonly referred to as "emission". However, the measurements carried out also allowed us to calculate two other, often neglected parameters of aeolian dust dynamics: gross emission and gross deposition. Gross emission is the total mass of sediment effectively worn away from the Earth's surface after a given time interval. Gross deposition, in its turn, is the total mass of sediment effectively depositing on the Earth's surface. Net emission is the difference between gross emission and gross deposition. Because during a wind erosion event some of the sediment emitted is replaced by freshly deposited sediment eroded upwind, net emission is always less then gross emission. Net emission is the final effect of the aeolian activity that took place. If it is positive then the sediment layer on the surface becomes thinner; if it is negative then the surface is nourished with sediment and the sediment layer thickens. In this perspective, net emission is the equivalent of negative accumulation.

A detailed, more fundamental study of gross emission, net emission and gross deposition based on the results of the Nellis Dunes measurements can be found in a scientific paper published in the journal Earth Surface Processes and Landforms (Goossens and Buck,

2010). A copy of that paper has been attached to this report (see Appendix B). In the current chapter we present the original data of the measurements, for this is what is needed to evaluate the role of wind erosion in the global dust production in NDRA. Readers interested in the more fundamental approach are referred to the published paper.

2. Dust dynamics by wind in the Nellis Dunes Recreation Area: methodology

2.1 Selection of dust stations

Dust dynamics were measured on all 17 surface units that occur in the Nellis Dunes area. Four dust stations were selected for each surface unit, 68 stations in total. For practical reasons (ability to collect all samples on a same day, which is necessary to compare stations and exclude effects caused by variations in atmospheric conditions) the stations were installed in 34 groups of two stations each. In each group the stations were installed in the same neighborhood, between 5 and 20 m from each other. There was no interference between the stations and each station can be considered an independent site, measuring its own dust dynamics. All data were calculated for each station individually, and the average result of the four stations installed on a same surface unit was calculated later. Data for the individual stations remain available and can be provided upon request.

Since the purpose of the measurements was to measure dust dynamics by wind erosion only, a special effort was made to install the stations in areas well away from zones of intense recreational use. This prevents local off-road vehicular activity (ORV) from affecting the results. Dust emitted by ORV activity has already been significantly diluted when arriving at a dust station, and its vertical concentration gradient will be close to zero because the medium-sized and coarse particles will have been removed from the cloud during transport. Because of the zero concentration gradient ORV-supplied dust does not affect the calculation of the local emission caused by wind erosion (see section 2.4 for more details).

The locations of the stations are shown in Fig. 1. The scale of the map does not allow showing the position of the two individual stations installed in a same neighborhood, therefore only the 34 neighborhoods are marked on the map.

2.2 Dust collection and analysis

Each dust station consisted of a 2-m long, 2-cm diameter metal pole to which 4 BSNE sediment samplers (Fryrear, 1986) were attached (Fig. 2). Airborne sediment was collected at the following heights: 25 cm, 50 cm, 75 cm and 100 cm. No collections were

performed at higher levels because the focus of the study was on erosion and deposition at or near ground level. BSNE samplers were used because (1) this type of sampler is widely used worldwide; (2) its efficiency for collecting particles has been determined over a wide particle range, from less than 10 µm up to 287 µm (Shao et al., 1993; Goossens and Offer, 2000; Goossens et al., 2000; Sharratt et al., 2007). Samples were collected over periods of 2 weeks each, from 19 December 2007 to 16 December 2008. Twenty-six periods were thus sampled. Two-week samplings were the minimum to collect enough dust for subsequent grain size and chemical analysis.

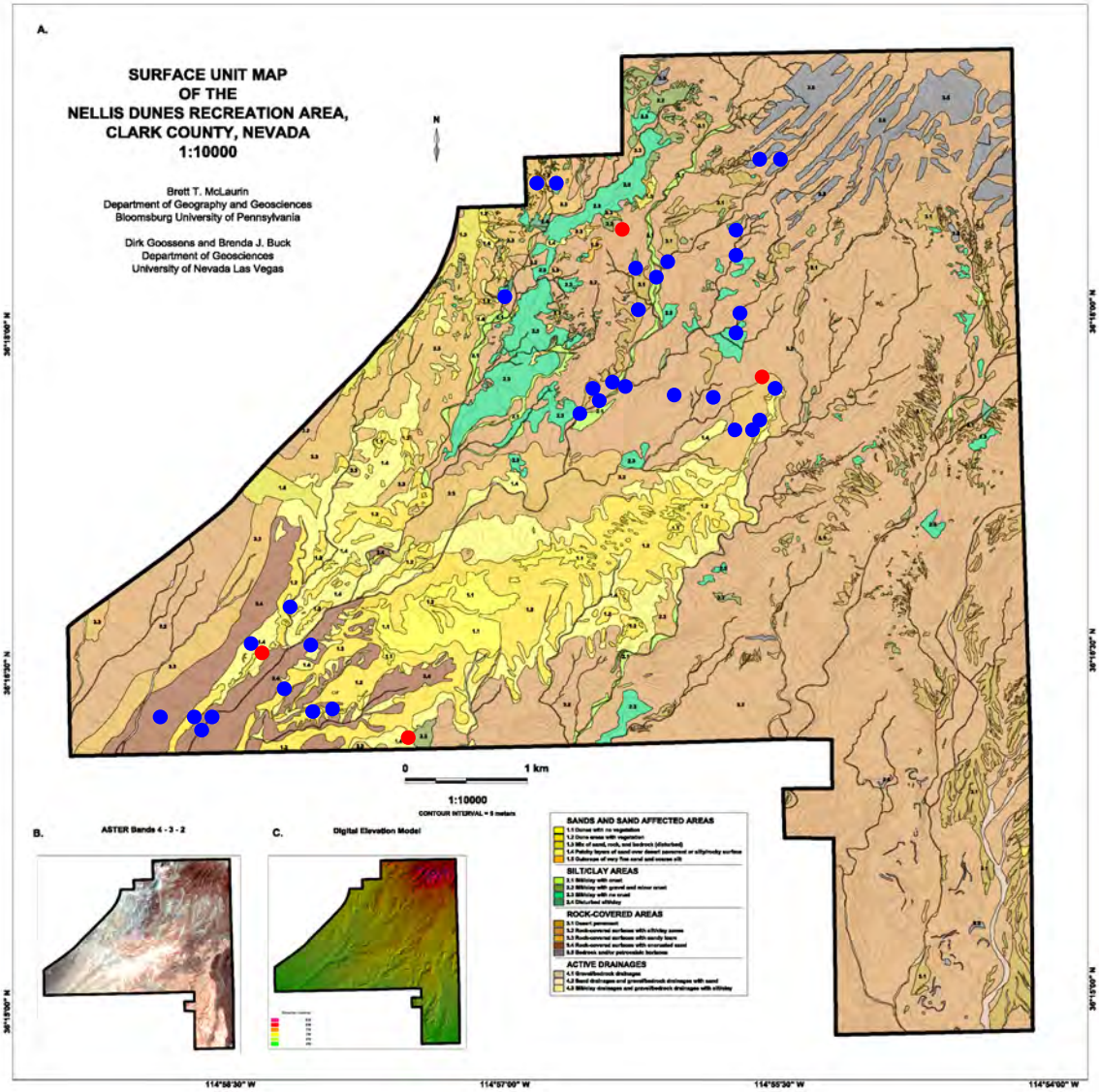

Fig. 1: Location of the wind erosion measurement sites (blue) and wind towers (red). Two dust stations were installed at each site.

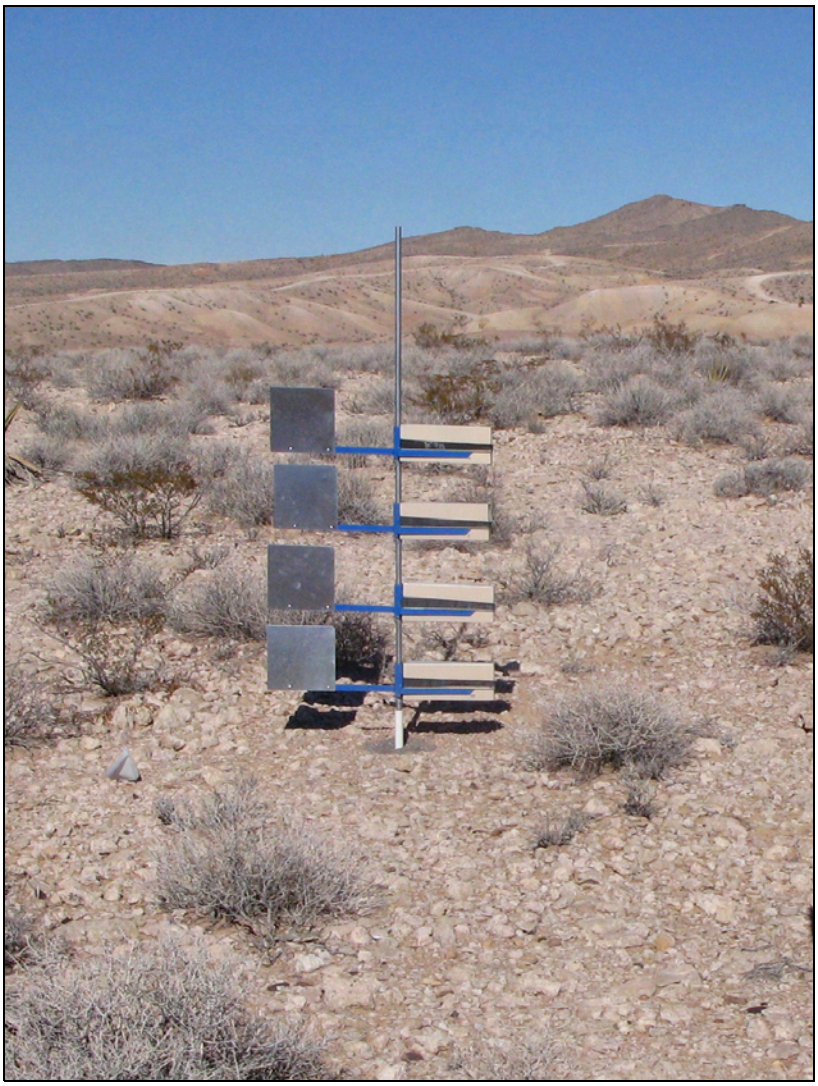

Fig. 2: Dust station with four BSNE dust collectors

After each period new, fresh samplers were installed and the used ones brought to the laboratory. Sediment was collected with a brush. Samples were weighed to a precision of 0.0001 g and subsequently analyzed for grain size distribution using a Malvern Mastersizer 2000 laser particle size analyzer (Malvern Instruments Ltd., Malvern, UK) in the Environmental Soil Analytical Laboratory at UNLV. Samples were initially analyzed in a water solution, but additional dry analyses were performed with a Malvern Mastersizer S instrument to determine the degree of dispersion during wet analysis. Some dispersion also occurred in a few samplers themselves during (rare) cases of rainfall during the measurements. All data were corrected for such dispersion using the information provided by the dry analyses.

Corrections for insplash of particles into the BSNEs during heavy rainfall were also performed. Comparisons of the mass of sediment collected at a same level and at identical airborne concentrations for splash and non-splash episodes showed that significant insplash only occurred in the lowermost two BSNEs; the uppermost two BSNEs were not significantly affected. Splash corrections were only necessary for a minority of collection periods.

2.3 Wind measurements

Three 20-m wind towers (Fig. 3) and one 10-m wind tower were erected in the Nellis Dunes area. Each cluster of dust stations contained at least one wind tower (see Fig. 1). Wind speed, wind direction and temperature data were collected as 1-h averages between 19 December 2007 and 16 October 2008 and as 10-min averages from 16 October 2008 to 16 December 2008. Data from the nearby Nellis Air Force Base meteorological station, which borders on the test field, were used to fill data gaps. Such gaps were filled only after careful calibration between the wind towers and the Nellis Air Force Base station.

Additional wind measurements were performed at all dust stations with a portable 3-m long wind tower containing 4 anemometers (heights: 56 cm, 121 cm, 202 cm and 259 cm) to determine the roughness length (z_0) and the wind profile near each pole (Fig. 4). In total, 396 periods of 10 min each were sampled with the portable tower. Wind speeds at all catcher levels (25 cm, 50 cm, 75 cm and 100 cm) were then calculated and linked to the data collected from the 4 wind towers. From this information it is possible to calculate the wind speeds and friction velocities required to determine erosion, for wind erosion only occurs at winds strong enough to create a neutral atmospheric boundary layer in the lowermost meters near the ground (see Turner, 1994). Under such circumstances the wind profile is logarithmic and there is no need for stability corrections. Since there was at least one wind tower close by each dust station and wind speed was measured at relatively high altitudes from each tower, and because the roughness length is known at each station, wind data can be reconstructed at all stations using the wind profile (logarithmic, as explained above) and the tower data. Comparing data collected by the portable tower to those reconstructed by the method explained above (Fig. 5) confirms the reliability of the technique.

2.4 Calculation of net emission

Various methods exist to calculate net erosion (emission) of soil dust. A review is given in a recent book by Shao (2008). Emission calculations based on airborne dust concentration data generally are more reliable than calculations based on airborne dust transport data because they are more direct; therefore we selected the former option to calculate net erosion in the Nellis Dunes area.

Fig. 3: 20-m wind tower with anemometer and wind vane

Fig. 4: Portable wind towers with four anemometers

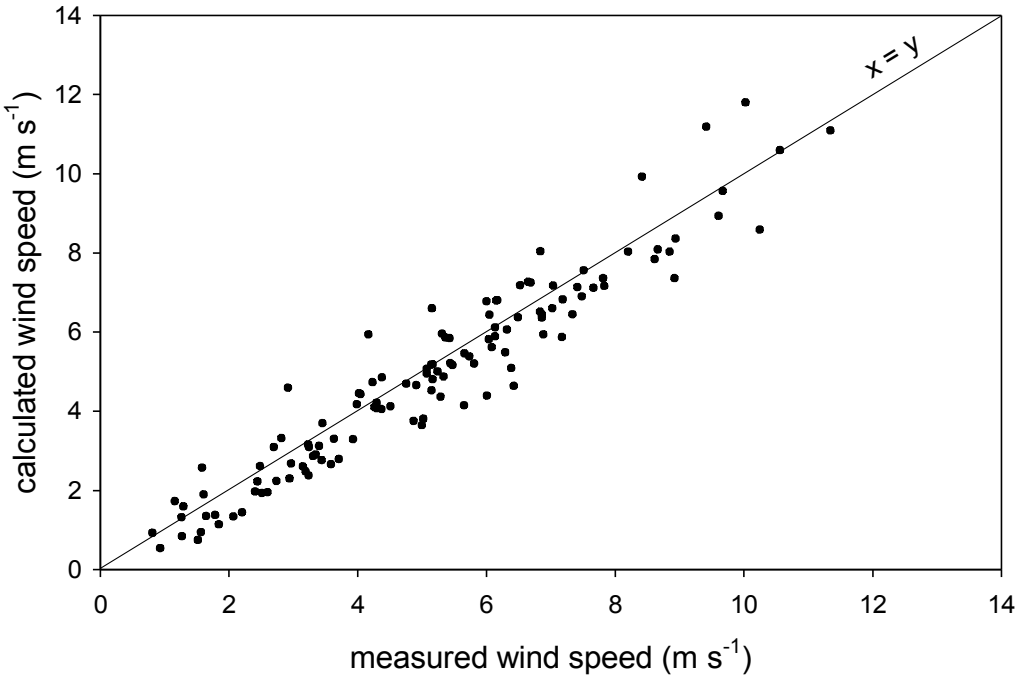

Fig. 5: Calculated *versus* measured wind speeds. Duration of test periods varied from 20 to 40 minutes. Each test period consisted of individual intervals of 10 minutes; 396 10-min intervals were measured in total.

Methods based on airborne concentration use vertical particle exchange to calculate vertical dust flux. Because this flux is affected by both the upward and downward movements of particles it always is an average flux; while in transport particles experience the effects of both velocity components. Also, they experience, simultaneously with the turbulent forces, the effect of gravity. Thus, numerical values of vertical dust flux collected from experiments always refer to net vertical flux; there is no need to add an extra term for deposition for the effect of deposition is already included in the experimentally recorded number.

Vertical dust flux can be calculated with Gillette's (1977) gradient method:

$$F = \frac{k \cdot u_* \cdot (C_1 - C_2)}{\ln(z_2 / z_1)} \tag{1}$$

where F = vertical dust flux, k = von Karman constant (0.4), u_* = friction velocity, and C_1 and C_2 = airborne dust concentrations at heights z_1 and z_2, respectively. This formula calculates the average vertical flux between heights z_1 and z_2; it does not calculate the erosion at ground level nor does it provide information on how the flux varies within the vertical layer bordered by z_1 and z_2. The latter problem can be solved by integrating the

original exchange formula for neutral atmospheric conditions (neutral because we apply it to episodes with active wind erosion), $F = -k \cdot u_* \cdot z \cdot \frac{\partial C}{\partial z}$, accepting that C varies with z as a power function $C = a \cdot z^b$ (see e.g. Nickling, 1978; Buschiazzo and Zobeck, 2005), where a and b are numerical constants. This leads to:

$$F = -k \cdot u_* \cdot a \cdot b \cdot z^b \tag{2}$$

This expression, which was first proposed by Goossens et al. (2001), allows calculating vertical dust flux at any arbitrary height z in the constant shear stress layer. For $b>0$, F is negative and the flux is directed downward; for $b<0$, F is positive and the flux is directed upward.

For calculating the flux at ground level, the best option is to construct the vertical flux profile and extrapolate it to zero level (Goossens et al., 2001; Hoffmann et al., 2008) for neither Gillette's gradient method and Goossens et al.'s integration methods provides a mathematical solution for $z = 0$. To do this, several options exist: (1) calculate the vertical flux for several separate layers using the gradient method, adjust each flux value to the average height of the corresponding layer, and extrapolate the profile to zero level (modified Gillette 1977 method); (2) use the gradient technique, but the vertical fluxes are calculated for layers bordered by the highest catcher (top) and each subsequent catcher underneath (bottom); the flux is then calculated as the average vertical flux for these layers (see Hoffmann et al., 2008); (3) calculate the vertical flux at a large number of elevations using the integration method and extrapolating the profile to zero level (Goossens et al., 2001); (4) calculate the vertical flux at only those elevations where the catchers are installed and extrapolate the profile to zero level. Comparative tests showed that the first and last option lead to similar results whereas those from the second option result in under-estimation and the third option results in an overestimation of the emission (Fig. 6). The first option has the disadvantage that it sometimes results in negative erosion results and that small experimental error in the measurements (which is inevitable) has major effects on the final result. Option 4 does not suffer from these problems and also exclusively uses original data; therefore this option was selected to calculate net erosion in the Nellis Dunes experiment.

All extrapolations were done by fitting a third order polynomial through the data points, which gave a variation coefficient $R^2 > 0.99$ for all stations. Visual inspections of the profiles were made to confirm the extrapolations.

The airborne dust concentrations C_z, necessary to calculate erosion, were calculated by dividing the horizontal transport flux F_h measured by the BSNEs by the wind speed (at each appropriate elevation). Average values were used for each 2-week period because all horizontal flux data are 2-week averages. All data were corrected for the efficiency of the BSNE using information from the calibration studies by Shao et al. (1993) and Goossens and Offer (2000).

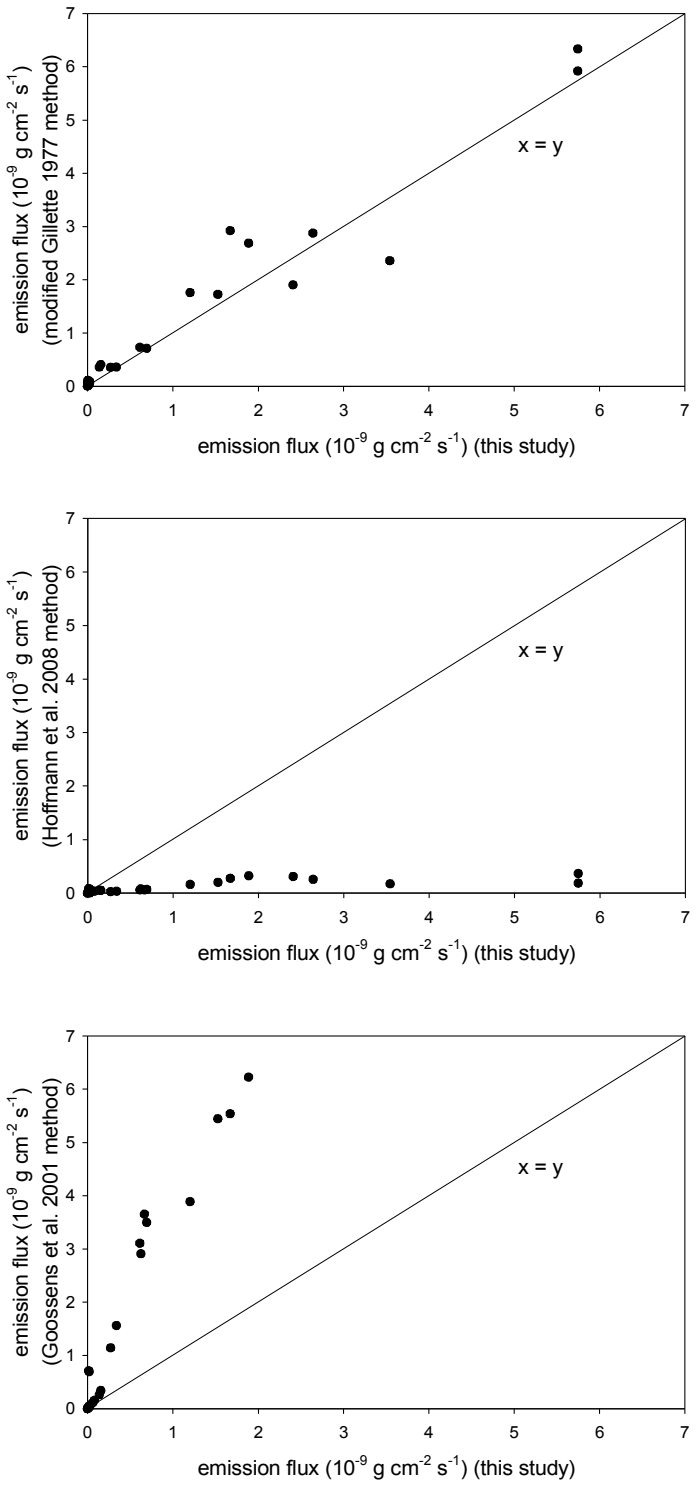

Fig. 6: Comparison of methods for extrapolating vertical dust flux to ground level. See text for explanation of each method.

The value of u_* in eq. (2) refers to the average friction velocity of the episodes of wind erosion; not the average u_* of all 14 days in each 2-week period. To determine the episodes of wind erosion we measured the deflation threshold (critical friction velocity at which wind erosion starts) with a Portable In Situ Wind Erosion Laboratory (PI-SWERL, see Chapter 4 of this report), at all dust stations. At least 4 measurements were done for each surface unit and the average deflation threshold was then calculated. To calculate the value of u_* in eq. (2), all 1-hour data from the 362-day long experiment were investigated and average friction velocities were calculated for each 2-week period by retaining only those u_* values that exceeded the deflation threshold. As 1-hour periods are still quite long for averaging friction velocities for the purpose of erosion calculations, we repeated the analysis for the period 16 October 2008 - 16 December 2008 for which 10-min data could be collected. Calculating the average friction velocities for 2-week intervals with these two options resulted in a difference of less than 3%, at all dust stations. Therefore, 1-hour data could be used for calculating u_* in eq. (2).

2.5 Calculation of gross deposition

Various techniques exist to calculate gross deposition. An overview, including comparisons between techniques, can be found in the study by Goossens and Rajot (2008). No direct measurements of dust deposition were performed in NDRA because (1) direct measurements of deposition at ground level usually suffer from local disturbances; (2) the proportion of dust in sediment deposited in sand areas (for instance, the sand dune units 1.1 and 1.2 in NDRA, see Chapter 2 for a description of the units) often is below the detection level of most grain size analyzers; and (3) the collection efficiency of dust deposition samplers heavily depends on wind speed and grain size, which affects the size distribution of collected dust (Goossens, 2007). Instead, dust deposition was calculated from the BSNE data using the inferential technique. This technique calculates deposition F_D as the product of airborne dust concentration C and the velocity of deposition v_d:

$$F_D = C \cdot v_d \tag{3}$$

In addition, comparative studies (e.g. Goossens and Rajot, 2008) showed that applying this technique to BSNE collections leads to deposition quantities identical to those measured with deposition catchers properly corrected for efficiency.

The velocity of deposition v_d, which is a function of particle size and shape and also depends on u_* and z_0, can be derived from standard graphs (see e.g. Sehmel, 1980), or it can be calculated from theoretical models (Sehmel and Hodgson, 1978; Slinn and Slinn, 1980; Slinn, 1983; Pleim et al., 1984; Venkatram and Pleim, 1999). Because these models assume that particles are spherical, which is a too simplified presumption for natural dust (see Goossens, 2007 or Goossens and Rajot, 2008 for examples), we used Dietrich's (1982) formula to calculate v_d. This formula includes a term for flattening

(*CSF*) and rounding (*P*) of grains and thus allows including particle shape in the calculations. For most types of soil-derived aeolian dust *CSF* and *P* are close to 0.70 and 3.45, respectively (Goossens, 2005); for the Nellis Dunes dust we used values of 0.69 and 3.47, which were derived from microscopic analysis of several dust samples. Strictly speaking Dietrich's formula does not calculate v_d but v_∞, the terminal settling velocity. For quartz grains in air and friction velocities below approximately 50 cm s^{-1} (typical values for the Nellis Dunes experiment reported here) the difference between v_d and v_∞ remains negligibly small once particles are coarser than 10 µm (see Sehmel, 1980). As the errors associated with particle shape are much larger than the difference between v_d and v_∞, Dietrich's approach was used. Comparisons of v_∞ and v_d calculated with Dietrich's and Slinn and Slinn's (1980) equations show that for (spherical, since Slinn and Slinn's formula applies to spheres) grains up to 50 µm the data are almost identical, and that for coarser grains the differences remain acceptable (Goossens and Rajot, 2008).

Velocities of deposition were initially calculated for 10 grain size fractions: 0-10 µm, 10-20 µm, 20-30 µm, 30-40 µm, 40-50 µm, 50-60 µm, 60-70 µm, 70-80 µm, 80-90 µm and 90-100 µm. Values for the mean particle size in each class (5 µm for the fraction 0-10 µm, 15 µm for the fraction 10-20 µm, etc.) were used when calculating deposition. In this report we regrouped the data into 3 classes: <20 µm, 20-60 µm and 60-100 µm. These 3 classes were selected based on the mode of transport of the particles: long-term suspension (<20 µm; particles can travel tens to hundreds of km after being released), short-term suspension (20-60 µm; particles usually travel several km to several tens of km after being released), and modified saltation (60-100 µm; particles usually travel several tens to at maximum several hundreds of m before settling to the surface again). Particles >100 µm were not considered in this study because most of these particles are transported in saltation, stay close to the surface, and do not create specific health problems.

To obtain gross (i.e., real) deposition, all data need to be recalculated to a perfectly absorbent surface. For aeolian deposition, water most probably is the best option currently available (Breuning-Madsen and Awadzi, 2005; Gigliotti et al., 2005; Goossens, 2005; Sow et al., 2006); therefore all deposition fluxes were recalculated to a water surface using the conversion factors provided by Goossens' (2005) study. Field measurements on dust deposition in SW Niger by Goossens and Rajot (2008) showed that this approach leads to very reliable results.

Gross deposition values were calculated at all 4 levels where BSNEs were installed (25, 50, 75 and 100 cm). To determine gross deposition at ground level, vertical deposition profiles were calculated and extrapolated to zero level. As with net erosion, a third order polynomial provided an excellent fit at all dust stations.

Note that the same dataset (concentrations measured with the BSNEs) is used for the calculations of gross deposition and net emission; this reduces the effect of experimental uncertainties when these two processes are compared.

2.6 Calculation of gross emission

Because net emission simply is the difference between gross emission and gross deposition, gross emission can be calculated as the sum of net emission and gross deposition:

$$E = e + S \tag{4}$$

where E = gross emission, e = net emission and S = gross deposition. Note that, once sediment has been emitted, S can eventually become superior to E if sediment emitted upstream is settling at a rate higher than the local erosion rate. If this happens, e is negative, which simply means that the surface is accumulating sediment.

3. Dust dynamics by wind in the Nellis Dunes Recreation Area: results and discussion

3.1 Role of surface units

3.1.1 Emission rates

The emission rates (in g cm^{-2} s^{-1}) for gross emission (E), gross deposition (S) and net emission (e) are displayed in Fig. 7 for the three grain size fractions investigated: <20 µm (sediment prone to long-term suspension), 20-60 µm (sediment prone to short-term suspension) and 60-100 µm (sediment prone to modified saltation). In general the patterns are very similar for E, S and e. This is understandable for E and S, for if lots of grains are released from the surface then many grains are available for sedimentation. The agreement between the patterns of E and e is less evident than it may look at first sight, especially because e is so much smaller than E and S. For the sediment fraction <20 µm the ratio e/E is still 0.553 (or 55.5 %); for the fraction 20-60 µm it is only 0.012 (or 1.2 %), and for the fraction 60-100 µm, 0.002 (or 0.2 %). This shows that the coarser the sediment is, the more hidden sediment dynamics takes place on the Earth's surface. We call it hidden because it is not recorded by classic wind erosion measurements, which only record the final (net) result. Many more grains are moving over the surface that can be derived from net emission measurements; most grains have just been displaced over the surface after the event has ceased without having been evacuated. For the <20 µm fraction gross emission is 1.8 times greater than the net emission. For the fraction 20-60

µm it is 82 times greater, and for the fraction 60-100 µm, it is 460 times greater. Net emission is thus very different from gross emission.

Looking at the differences between the surface units, we see that the most active units (highest emission and sedimentation rates) are the sand substrata of units 1.1 to 1.5, and also, though somewhat less, the rock-covered sands of unit 3.4. Silt and drainage areas are much less active, at least in terms of mass. These conclusions apply to all 3 grain size classes but the dominance of the sand dunes (units 1.1 and 1.2) is particularly clear for dust transported in modified saltation (60-100 µm). For medium-sized silt (20-60 µm) the sandy drainages of unit 4.2 also show high aeolian activity.

The data for net emission are summarized in Table 1. All numbers are positive, which means that all 17 surface units in the Nellis Dunes area are net-emissive: there is always more emission than deposition; all units are characterized by a negative sedimentation

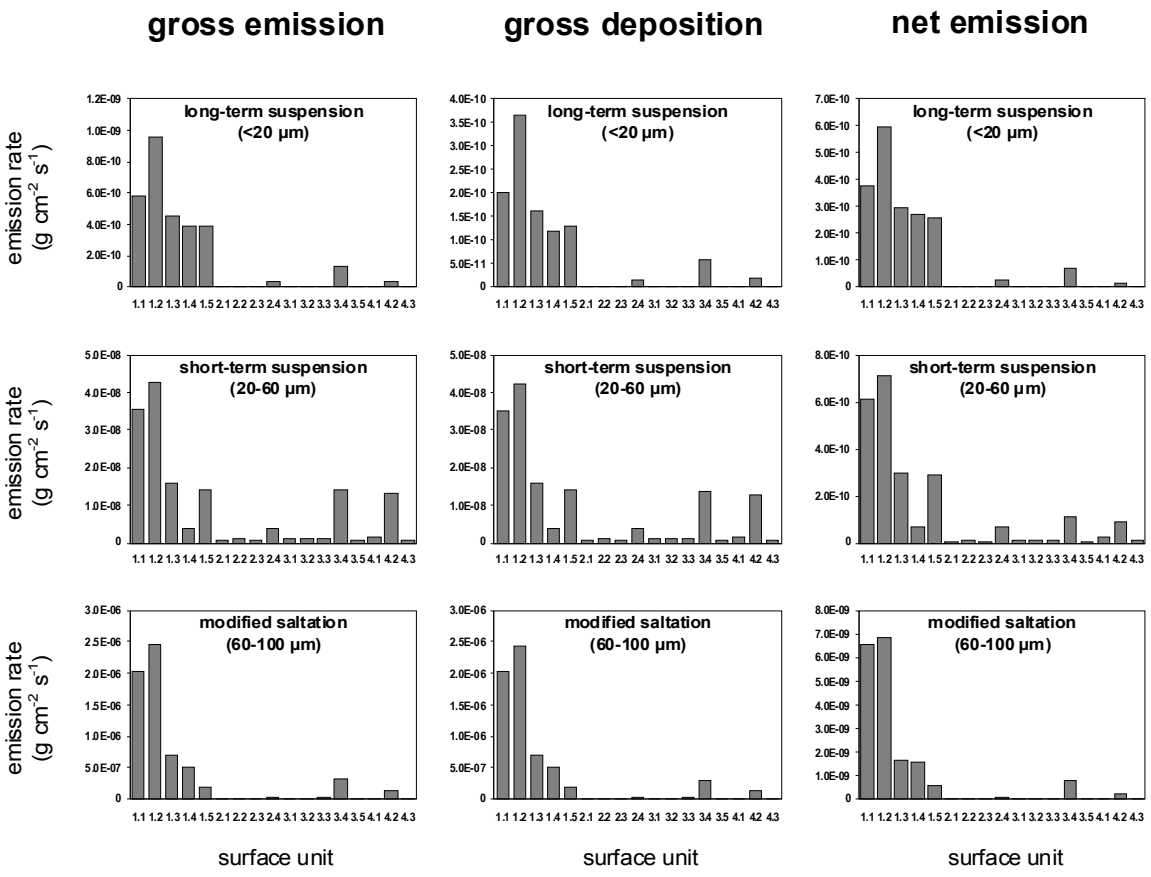

Fig. 7: Emission rates for gross emission, gross deposition and net emission for sediment prone to long-term suspension (<20 µm), short-term suspension (20-60 µm) and modified saltation (60-100 µm).

Table 1: Net emission rates for dust emission by wind erosion for the 17 surface units, for sediment prone to long-term suspension (<20 µm), short-term suspension (20-60 µm) and modified saltation (60-100 µm).

surface unit	net emission rate by wind erosion (g m^{-2} $year^{-1}$)		
	<20 µm (long-term suspension)	20-60 µm (short-term suspension)	60-100 µm (modified saltation)
1.1	118.32	193.44	2059.51
1.2	188.37	224.44	2169.64
1.3	92.94	92.90	506.17
1.4	85.32	22.83	484.21
1.5	81.84	92.75	184.79
2.1	0.23	1.52	2.56
2.2	1.03	4.23	3.34
2.3	0.60	1.70	1.21
2.4	7.96	21.19	24.33
3.1	0.60	3.54	3.98
3.2	0.31	3.09	4.28
3.3	0.48	3.03	7.85
3.4	23.58	36.10	242.02
3.5	0.17	1.56	1.50
4.1	1.70	8.66	6.76
4.2	5.74	29.22	57.53
4.3	0.48	2.74	3.46
sandy surfaces	113.36	125.27	1080.86
silty surfaces	2.46	7.16	7.86
rock-covered surfaces	5.03	9.46	51.93
drainages	2.64	13.54	22.59

balance. The large differences between the units are obvious from the table. The most emissive units (in terms of mass) are the sand substrata (units 1.x), followed by the rock-covered substrata (units 3.x) and the drainages (units 4.x). Silt substrata (units 2.x) are the least emissive. The high emission rates of the sand surfaces during natural wind conditions are explained by the loose and cohesionless structure of the top layer and the many saltating sand grains, which act as an initiator for releasing finer particles (Shao, 2008). Rock-covered silt substrata are less homogeneous than rock-free silts, the rock fragments increase the degree of turbulence near the ground promoting emission, and biological activity near and underneath the clasts produces loose aggregates vulnerable to emission. Drainages, finally, are more cohesive that their dry equivalent due to the precipitation of soluble carbonates and salts imported from surrounding regions during runoff. These substances bind the grains once the water has evaporated, creating protective crusts or cements.

3.1.2 Annual emissions by wind erosion in NDRA

The data in section 3.1.1 show the emission (or sedimentation) rates, i.e. the vulnerability of the surface units to the parameter (emission or sedimentation) in question. The current section investigates the effective productivity of the units. Effective productivity does not only depend on the emission and deposition rates, but is also determined by the areal extent of the units. Units with a high emission rate may be marginal suppliers of dust if they cover only small surfaces, and units with relatively low emission rates may still produce significant amounts if they are very abundant. This section investigates which units are the greatest suppliers of dust when wind erosion takes places in the Nellis Dunes Recreation Area.

The absolute amounts of dust gross emitted, gross deposited and net emitted annually in the Nellis Dunes area (in tons per year) are displayed in Fig. 8 for the three grain size fractions investigated (<20 μm, 20-60 μm and 60-100 μm). As with the emission rates the patterns are very similar for *E*, *S* and *e* for each fraction. The parameter of most interest for management purposes is net emission, and this parameter is described in more detail below.

During natural wind erosion by far most dust in NDRA is (net) emitted in the loose, uncompacted sand units 1.1 to 1.4. The most productive areas are the partly vegetated sand dunes (unit 1.2). The unvegetated dunes (1.1) produce significantly less dust, not only because they cover an area more than 4 times smaller that the partly vegetated dunes but also because they are more active and have lost a significant portion of their fine particles over time, leading to a much lower dust content in the top layer compared to the vegetated dunes that are less frequently prone to wind erosion (Fig. 9). All silt units, though very rich in dust, do not significantly contribute to net dust production in NDRA during wind erosion because their top layer is stabilized by surface crusts and/or rock cover. Even unit 3.2 (rock-covered silt and clay), which is by far the most abundant unit and covers more than 56 % of the NDRA, does not contribute significantly to the dust load in the Nellis Dunes area. Only for medium-sized dust (20-60 μm) is this unit a significant supplier of dust (Fig. 8). Unit 3.4, which is very similar to unit 3.2 except that it contains much more sand, produces even more dust than unit 3.2 despite it is 15 times less abundant and is commonly characterized by a cyanobacterial crust. The other sand unit characterized by a surface crust (unit 1.5, mixture of sand and fine silt) is not an important supplier of dust during natural wind erosion in the NDRA because of its very limited occurrence (only 0.1 % of the surface of NDRA).

The amounts of dust (net) emitted annually in NDRA are shown in Table 2. The large differences between the units are prominent. An interesting observation is that the numbers for the <20 μm and 20-60 μm fractions are almost identical (859 ton and 935 ton respectively) despite the much larger particles of the latter fraction. If all grains would be perfectly spherical, then it can be calculated that the number of <20 μm particles net

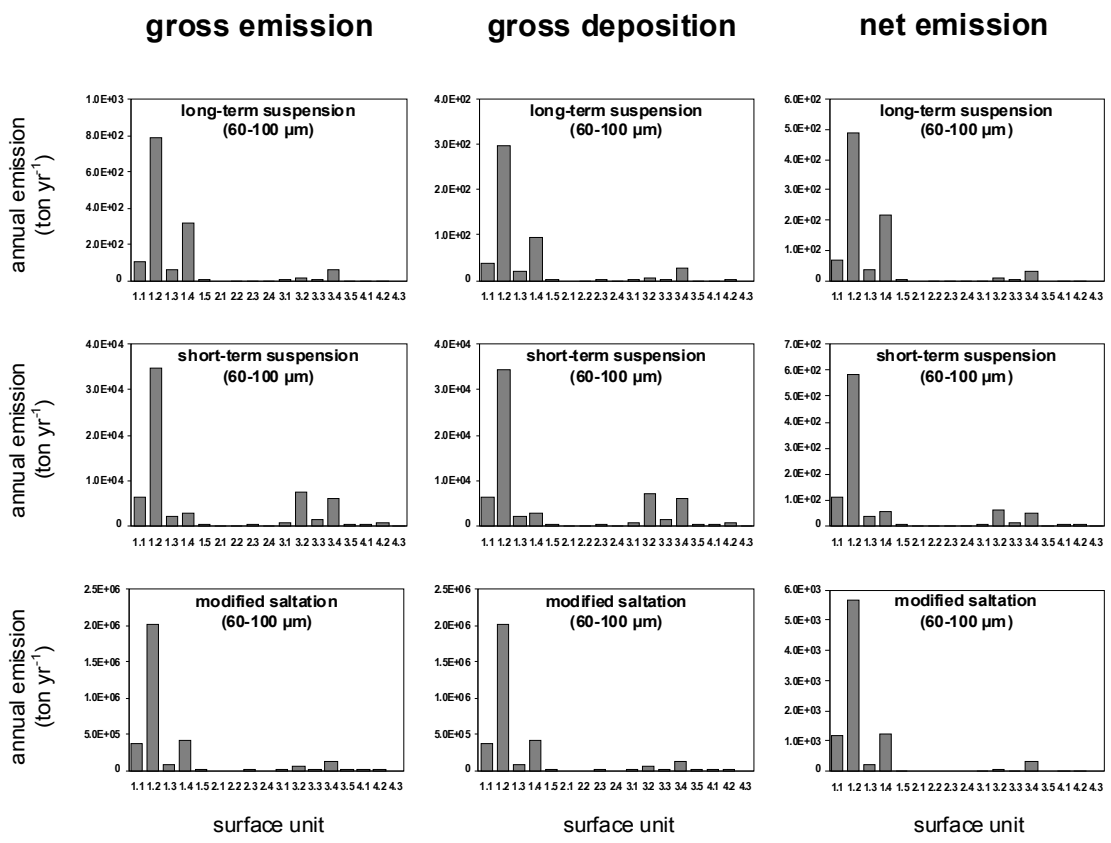

Fig. 8: Annual amounts of dust gross emitted, gross deposited and net emitted in the Nellis Dunes area in 2008, for sediment prone to long-term suspension (<20 µm), short-term suspension (20-60 µm) and modified saltation (60-100 µm).

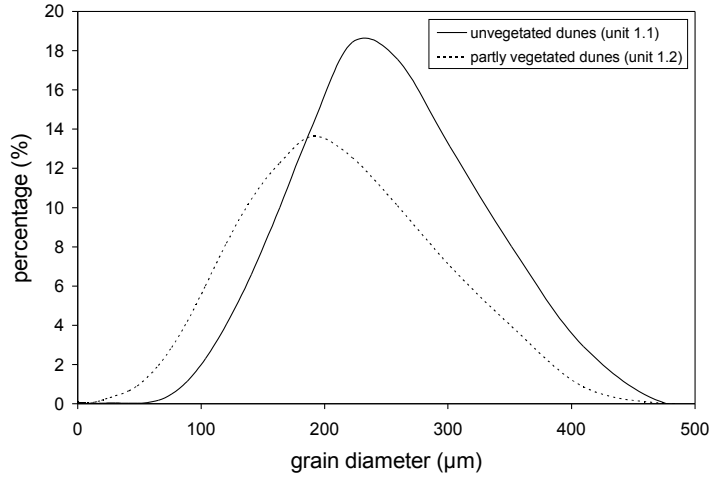

Fig. 9: Grain size distribution of the top soil (upper cm) in unvegetated and partly vegetated dunes at NDRA

Table 2: Annual amounts of dust net emitted in NDRA by wind erosion for the 17 surface units, for sediment prone to long-term suspension (<20 µm), short-term suspension (20-60 µm) and modified saltation (60-100 µm).

surface unit	emission amounts (ton yr^{-1})		
	<20 µm (long-term suspension)	20-60 µm (short-term suspension)	60-100 µm (modified saltation)
1.1	68.02	111.21	1184.00
1.2	489.10	582.76	5633.40
1.3	37.08	37.07	201.98
1.4	217.24	58.12	1232.83
1.5	3.02	3.42	6.82
2.1	0.06	0.42	0.70
2.2	0.43	1.75	1.38
2.3	0.66	1.89	1.34
2.4	0.35	0.93	1.07
3.1	0.95	5.63	6.33
3.2	6.28	63.52	87.99
3.3	1.49	9.38	24.29
3.4	32.35	49.53	332.04
3.5	0.18	1.61	1.55
4.1	0.65	3.32	2.59
4.2	0.72	3.68	7.24
4.3	0.11	0.65	0.83
NDRA	858.70	934.87	8726.38

emitted in NDRA is 59 times larger than the number of net emitted 20-60 µm particles. The number of net emitted 60-100 µm particles is almost identical as for 20-60 µm particles (only 1.17 times higher). Therefore, on an annual basis, most particles net emitted by wind in NDRA are evacuated in long-term suspension.

3.2 Seasonal patterns

3.2.1 Net emission

The seasonal evolution of (net) emission in NDRA is shown in Fig. 10 for each of the four categories of surface units: sandy surfaces (units 1.1 to 1.5), silty surfaces (units 2.1 to 2.4), rock-covered surfaces (units 3.1 to 3.5) and drainages (units 4.1 to 4.3). Because the emission values can strongly differ within the same surface group, it is necessary to normalize the data; otherwise the patterns for the most active units would obscure those

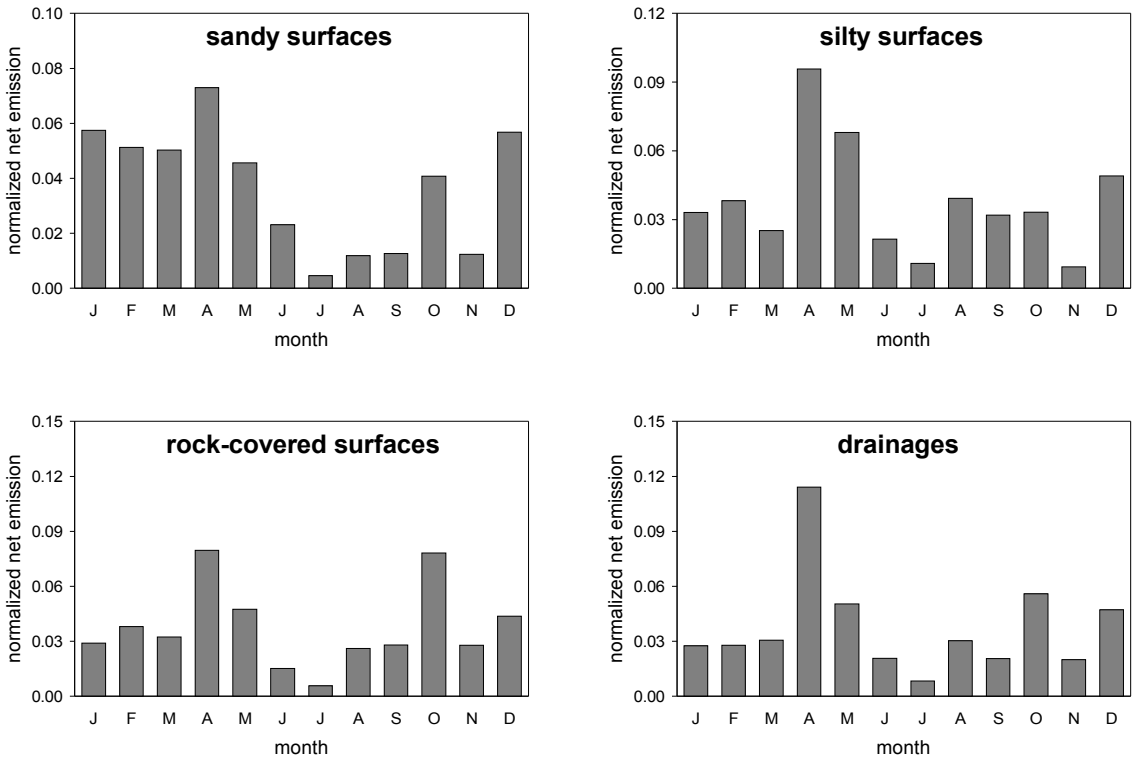

Fig. 10: Seasonal evolution of net emission in NDRA for the four categories of surfaces: sandy surfaces (units 1.1 to 1.5), silty surfaces (units 2.1 to 2.4), rock-covered surfaces (units 3.1 to 3.5), and drainages (units 4.1 to 4.3). Data are for total suspendable dust (0-60 μm).

of the slightly active units. All data were normalized by setting the annual average net emission equal to unity for all surface units. This does not affect the shape of the diagrams.

The patterns for the various size fractions were almost identical; in Fig. 10 we show the data for the total suspendable dust fraction (0-60 μm) as an example.

There is a clear difference between the sandy surfaces on the one hand and the three other types of surfaces on the other. The silty, rocky and drainage surfaces shown identical patterns with the highest net emission in the spring (April-May) and the lowest emission in summer (June-July). In the remaining months net emissions are fairly constant (the high value in October was caused by an only 1-h long, but very heavy storm on October 5). The sandy surfaces behave differently in that they are also highly emissive in the winter months (December-March) when the other surfaces are relatively stable. The contrast between winter-spring and summer-fall is much more pronounced for surfaces containing sand than for other surface types. The effect of the October 5 storm is clearly visible in the sand diagram but does not affect the general trend.

Although the diagrams are still somewhat irregular due to the relatively short duration (only one year) of the measurements we can still make the following important observations: the most dust in NDRA emitted by natural wind erosion occurs in the spring (and winter for sandy surfaces) whereas the smallest emissions occur in the summer, especially in the period June-July.

3.2.2 Evacuation rate

The rate at which sediment is evacuated during wind erosion can be quantified by the ratio of gross deposition to gross emission, *S*/*E*. For example, if *S*/*E* = 0.90 then 90 % of the eroding particle mass is replaced with freshly settling grains eroded upwind; 10 % of the mass is not replaced and will be evacuated from the spot in question. Especially the finest particle fractions, which are transported in long-term suspension and do not rapidly return to the surface, can be expected susceptible to evacuation.

Fig. 11 shows how the evacuation of dust from NDRA varies throughout the year for each of the four categories of surfaces. Here too the data were normalized to allow displaying all surface groups in a single diagram. The pictures for the various size fractions were nearly identical; we show the data for the total suspendable dust fraction (0-60 µm) as an example.

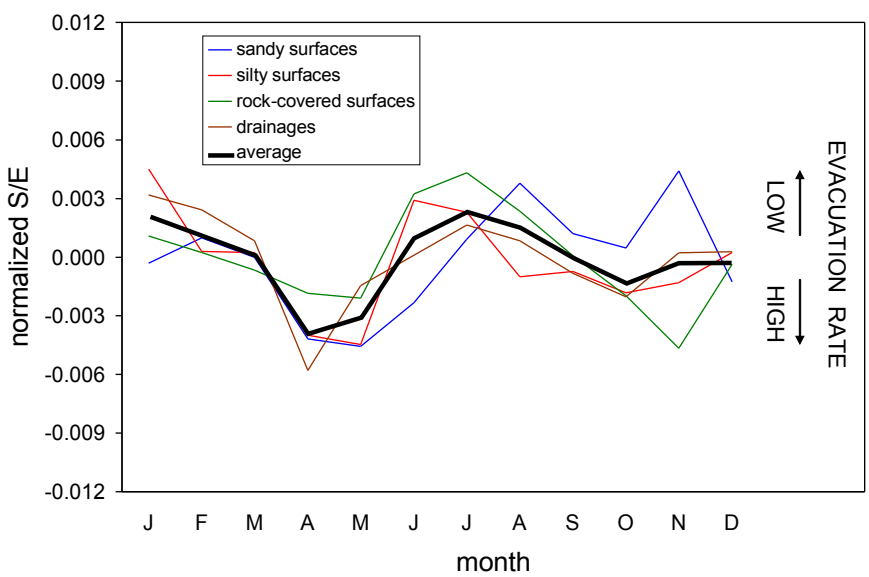

Fig. 11: Seasonal evolution of dust evacuation rate in NDRA for the four categories of surfaces: sandy surfaces (units 1.1 to 1.5), silty surfaces (units 2.1 to 2.4), rock-covered surfaces (units 3.1 to 3.5), and drainages (units 4.1 to 4.3). Data are for total suspendable dust (0-60 µm).

The evacuation rate is highest (low *S/E*) in spring (April-May) and in the fall (October), and lowest (high *S/E*) in summer (June-August) and in winter (January-February). To better interpret this pattern we calculated the evacuation rate as a function of dust activity. In NDRA dust transport is highest from mid April to mid May, lowest from mid July to mid February, and intermediate in the remaining months (Fig. 12A). Plotting *S/E* for each of these three periods separately (Fig. 12B) we see that the stronger the dust activity, the higher (low *S/E*) the evacuation becomes. During active periods dust emitted will settle less easily to the surface again; it will remain better suspended in the atmosphere and more easily evacuated from the Nellis Dunes area. This behavior is directly correlated to the wind speed (see Fig. 12C), for the stronger the wind blows the higher dust activity is and the higher the upward velocity fluctuations of the wind vector become, keeping the particles better aloft.

3.2.3 Grain size

To get an idea of the seasonal evolution of the size of the dust emitted from NDRA we calculated the median grain diameter (D50) of the airborne sediment and plotted it in Fig. 13A. Here too the temporal evolutions were very similar for all grain size fractions; Fig. 13A shows the curves for the total suspendable dust fraction (0-60 µm) as an example. Airborne dust was coarsest in winter (December-February) and then became finer until November. Local peaks of somewhat coarser dust do occur, but do not mask the general trend. However, the most important conclusion is that dust emitted from sand areas is considerably finer than dust emitted from silty areas, and certainly finer than dust emitted from rock-covered areas and drainages (Fig 13A). The difference is substantial: the annual average median grain diameters are 33 µm (sand areas), 38 µm (silt areas), 41 µm (rock-covered areas) and 40 µm (drainages). Two mechanisms may explain this behavior. First, the sand areas are much more active than the other areas. Over time they have lost a significant proportion of their most erodible fractions and in contrast to the other units, which can replace these fractions from underlying silty reservoirs, replacement of coarse silt (the most erodible fraction) is difficult. Therefore, in the total suspendable fraction, the proportion of coarse silt is smaller in the dunes and the median grain diameter of the suspendable dust will be lower. Secondly, in sand areas most dust emission is caused by impacting saltating grains. Fine particles that would normally not be released because they are sticking to other grains may now become emitted upon impact, resulting in a smaller median grain diameter in the cloud of emitted grains.

There is a tendency for the emitted dust to be somewhat coarser during periods of higher emission. To illustrate this we plotted the median grain diameter (for the total suspendable fraction, as before) as a function of the net emission rate (Fig. 13B). Although not very spectacular the trend is easily discernable in the diagram. High net emissions are associated with high wind speeds, which facilitate the emission of coarser grains.

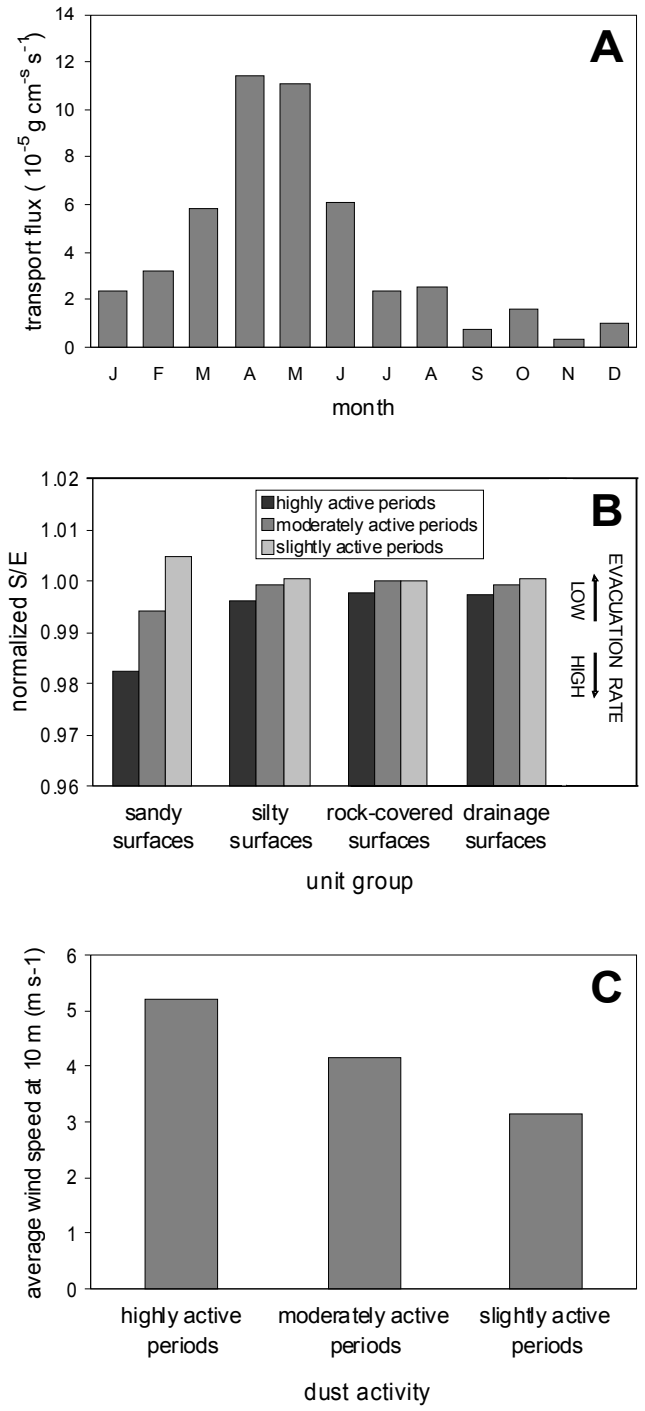

Fig. 12: Dust evacuation rate as a function of dust activity. (A) dust transport at NDRA; (B) normalized evacuation rate for highly active, moderately active and slightly active periods, for the four categories of surfaces; (C) average wind speed at 10 m. See text for criteria. Data are for total suspendable dust (0-60 μm).

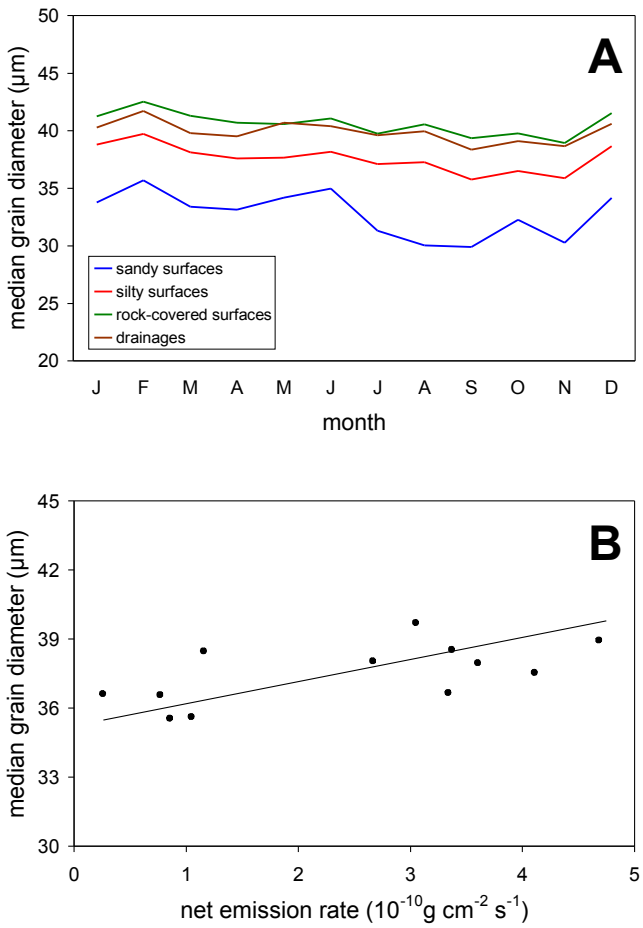

Fig. 13: Grain size of airborne dust at NDRA. (A) seasonal evolution of the median grain diameter for total suspendable dust (0-60 µm), average for the four sampling heights of 25 cm, 50 cm, 75 cm and 100 cm; (B) median grain diameter for total suspendable dust as a function of the net emission rate.

4. Summary of conclusions

All 17 surface units in the Nellis Dunes area are net-emissive: there is always more emission than deposition. All units are thus characterized by a negative sedimentation balance.

The units most vulnerable to dust emission during natural wind erosion are the sand substrata, followed by the rock-covered substrata and the drainages. Silt substrata with no or only sparse rock fragments are the least emissive surfaces. The high emission rates of the sand substrata are explained by the loose and cohesionless structure of the top layer

and the many saltating sand grains, which act as an initiator for releasing finer particles. Rock-covered silt substrata are less homogeneous than rock-free silts; the rock fragments increase the degree of turbulence near the ground promoting emission, and biological activity near and underneath the clasts produces loose aggregates vulnerable to emission. Drainages, finally, are more cohesive due to the precipitation of soluble carbonates and salts imported from surrounding regions during runoff. These substances bind the grains once the water has evaporated, creating protective crusts or cements.

During wind erosion by far most dust in NDRA is emitted from the loose, uncompacted sand units 1.1 to 1.4. The most productive areas are the partly vegetated sand dunes (unit 1.2). The unvegetated dunes (unit 1.1) produce significantly less dust. All silt units, though very rich in dust, do not significantly contribute to net dust production in NDRA during wind erosion because their top layer is stabilized by surface crusts and/or rock cover. Unit 1.5 (mixture of sand and fine silt) is not an important supplier of dust in the NDRA because of its very limited occurrence (only 0.1 % of the surface of NDRA) and because it is characterized by a physical surface crust.

The silty, rocky and drainage surfaces produce most dust in the spring (April-May) and much less dust in summer (June-July). The sandy surfaces behave differently in that they are also highly emissive in the winter months (December-March) when the other surfaces are relatively stable. The contrast between winter-spring and summer-fall is much more pronounced for surfaces containing sand than for other surface types.

In NDRA most dust transport from natural wind erosion takes place from mid April to mid May. Dust transport is low from mid July to mid February, and intermediate in the remaining months. The evacuation rate is highest in spring (April-May) and in the fall (October), and lowest in summer (June-August) and in winter (January-February).

Periods of high evacuation rates are associated with periods of high dust activity. During active periods the emitted dust settles less easily to the surface, remains better suspended in the atmosphere and is more easily evacuated from the Nellis Dunes area. This behavior is directly correlated to the wind speed. The stronger the wind blows, the higher dust activity is and the higher the upward velocity fluctuations of the wind vector become keeping the particles better aloft.

Airborne dust in NDRA is coarsest in winter (December-February) and gets finer until November. Dust emitted from sand areas is considerably finer than dust emitted from silty areas, and even finer than dust emitted from rock-covered areas and drainages. One reason is that the sand areas are much more active than the other areas. Over time they have lost a significant proportion of their most erodible fractions (coarse silt) and in contrast to the other units, which can replace these fractions from underlying silty reservoirs, replacement of coarse silt is difficult. This results into a smaller median grain diameter in the dunes. A second reason is that in sand areas most dust emission is caused by impacting saltating grains. Fine particles that would normally not be released because

they are sticking to other grains may now become emitted upon impact, resulting in a smaller median grain diameter in the cloud of emitted grains.

Dust emitted from NDRA is coarsest during periods of strong wind erosion. High net emissions are associated with high wind speeds, which facilitate the emission of coarser grains.

Acknowledgement

D. Pepper and U. Rangegowda (College of Engineering, University of Nevada Las Vegas, Las Vegas, NV, USA) and X. Wang (Purdue University Calumet, Hammond, IN, USA) organized the collection of wind data from the wind towers and performed the initial processing of the wind records. V. Etyemezian and G. Nikolich (Desert Research Institute, Las Vegas, NV, USA) provided the portable wind tower and processed the raw data. Wind data from the Nellis Air Force Base meteorological station were provided by M. EmelyPoynter (Nellis Air Force Base, Las Vegas, NV, USA).

References

Breuning-Madsen, H., Awadzi, T.W., 2005. Harmattan dust deposition and particle size in Ghana. Catena 63, 23-38.

Buschiazzo, D.E., Zobeck, T.M., 2005. Airborne horizontal mass flux calculated with different equations. Proc. 2005 ASAE Annual Meeting, Tampa, Florida, USA, Paper No. 052049.

Dietrich, W.E., 1982. Settling velocity of natural particles. Water Resources Research 18**,** 1615-1626.

Fryrear, D.W., 1986. A field dust sampler. Journal of Soil and Water Conservation 41**,** 117–120.

Gigliotti, C.L., Totten, L.A., Offenberg, J.H., Dachs, J., Nelson, E.D., Reinfelder, J., Eisenreich, S.J., 2005. Atmospheric concentrations and deposition of polycyclic aromatic hydrocarbons to the mid Atlantic east coast region. Environmental Science & Technology 39**,** 5550-5559.

Gillette, D.A., 1977. Fine particulate emissions due to wind erosion. Transactions of the ASAE 20, 890-897.

Goossens, D., 2005. Quantification of the dry aeolian deposition of dust on horizontal surfaces: an experimental comparison of theory and measurements. Sedimentology 52, 859-873.

Goossens, D., 2007. Bias in grain size distribution of deposited atmospheric dust due to the collection of particles in sediment catchers. Catena 70, 16-24.

Goossens, D., Buck, B., 2010. Gross erosion, net erosion and gross deposition of dust by wind: field data from 17 desert surfaces. Earth Surface Processes and Landforms, doi: 10.1002/esp.2080.

Goossens, D., Offer, Z.Y., 2000. Wind tunnel and field calibration of six aeolian dust samplers. Atmospheric Environment 34, 1043-1057.

Goossens, D., Rajot, J.L., 2008. Techniques to measure the dry aeolian deposition of dust in arid and semi-arid landscapes: a comparative study in West Niger. Earth Surface Processes and Landforms 33, 178-195.

Goossens, D., Gross, J., Spaan, W., 2001. Aeolian dust dynamics in agricultural land areas in Lower Saxony, Germany. Earth Surface Processes and Landforms 26, 701-720.

Goossens, D., Offer, Z.Y., London, G., 2000. Wind tunnel and field calibration of five aeolian sand traps. Geomorphology 35, 233-252.

Hoffmann, C., Funk, R., Li, Y., Sommer, M., 2008. Effect of grazing on wind driven carbon and nitrogen ratios in the grasslands of Inner Mongolia. Catena 75, 182-190.

Nickling, W.G., 1978. Eolian sediment transport during dust storms: Slims River Valley, Yukon Territory. Canadian Journal of Earth Sciences 15, 1069-1084.

Pleim, J.E., Venkatram, A., Yamartino, R., 1984. ADOM/TADAP Model Development Program, vol. 4: The Dry Deposition Module. Ontario Ministry of Environment, Rexdale.

Sehmel, G.A., 1980. Particle and gas dry deposition: a review. Atmospheric Environment 14, 983-1011.

Sehmel, G.A., Hodgson, W.H., 1978. A Model for Predicting Dry Deposition of Particles and Gases to Environmental Surfaces. DOE Report PNL-SA-6721, Pacific Northwest Laboratories, Richland, WA.

Shao, Y., 2008. Physics and Modelling of Wind Erosion (2nd Ed.). Springer Science + Business Media B.V., Dordrecht.

Shao, Y., McTainsh, G.H., Leys, J.F., Raupach, M.R., 1993. Efficiencies of sediment samplers for wind erosion measurement. Australian Journal of Soil Research 31, 519-532.

Sharratt, B., Feng, G., Wendling, L., 2007. Loss of soil and PM10 from agricultural fields associated with high winds on the Columbia Plateau. Earth Surface Processes and Landforms 32, 621-630.

Slinn, W.G.N., 1983. Air-to-sea transfer of particles. In: Liss, P.S., Slinn, W.G.N. (Eds.), Air–Sea Exchange of Gases and Particles. NATO ASI Series, Reidel, Dordrecht, 299-405.

Slinn, S.A., Slinn, W.G.N., 1980. Predictions for particle deposition on natural waters. Atmospheric Environment 14, 1013-1016.

Sow, M., Goossens, D., Rajot, J.L., 2006. Calibration of the MDCO dust collector and of four versions of the inverted frisbee dust deposition sampler. Geomorphology 82, 360-375.

Turner, D.B., 1994. Workbook of Atmospheric Dispersion Estimates: An Introduction to Dispersion Modeling. Lewis Publishers, Boca Raton.

Venkatram, A., Pleim, J., 1999. The electrical analogy does not apply to modeling dry deposition of particles. Atmospheric Environment 33, 3075-3076.